Three-Dimensional Distribution of Transverse Collagen Fibers in the Anterior Human Corneal Stroma

Moritz Winkler,[1] Golroxan Shoa,[1] Yilu Xie,[2] Steven J. Petsche,[3] Peter M. Pinsky,[3] Tibor Juhasz,[1,2] Donald J. Brown,[2] and James V. Jester[1,2]

[1]Department of Biomedical Engineering, University of California, Irvine, California
[2]Gavin Herbert Eye Institute, University of California, Irvine, California
[3]Department of Mechanical Engineering, Stanford University, Stanford, California

Correspondence: James V. Jester, 843 Health Sciences Road, Hewitt Hall, Room 2036, University of California, Irvine, Irvine, CA 92697-4390; jjester@uci.edu.

Submitted: August 27, 2013
Accepted: October 3, 2013

Citation: Winkler M, Shoa G, Xie Y, et al. Three-dimensional distribution of transverse collagen fibers in the anterior human corneal stroma. *Invest Ophthalmol Vis Sci*. 2013;54:7293–7301. DOI:10.1167/iovs.13-13150

Purpose. Recent investigations of human corneal structure and biomechanics have shown that stromal collagen fibers (lamellae) are organized into a complex, highly intertwined three-dimensional meshwork of transverse oriented fibers that increases stromal stiffness and controls corneal shape. The purpose of this study was to characterize the three-dimensional distribution of transverse collagen fibers along the major meridians of the cornea using an automated method to rapidly quantify the collagen fibers' angular orientation.

Methods. Three eyes from three donors were perfusion-fixed under pressure, excised, and cut into four quadrants. Quadrants were physically sectioned using a vibratome and scanned using nonlinear optical high-resolution macroscopy. Planes were analyzed numerically using software to identify collagen fiber angles relative to the corneal surface, stromal depth, and radial position within the anterior 250 μm of the stroma.

Results. The range of fiber angles and the fiber percentage having an angular displacement greater than ±3.5° relative to the corneal surface ("transverse fibers") was highest in the anterior stroma and decreased with depth. Numerical analysis showed no significant differences in fiber angles and transverse fibers between quadrants, meridians, and radial position.

Conclusions. These results match our previous observation of a depth-dependent gradient in stromal collagen interconnectivity in the central cornea, and show that this gradient extends from the central cornea to the limbus. The lack of a preferred distribution of angled fibers with regard to corneal quadrant or radial position likely serves to evenly distribute loads and to avoid the formation of areas of stress concentration.

Keywords: cornea, corneal collagen, biomechanics, second harmonic generation imaging, collagen fiber organization

The human cornea serves both as a protective outer cover to the eye and as the primary refractive element responsible for focusing light back to the retina. Its primary structural and mechanical element is the corneal stroma, comprising over 90% of corneal thickness. The stroma itself is made up primarily of collagen, which accounts for about 70% of the corneal total dry weight.[1] Collagen molecules assemble into long fibrils that in the human cornea exhibit a uniform diameter of approximately 31 to 34 nm.[2] Their spacing, size, and stability are regulated by a combination of collagens and proteoglycans generating an interfibrillar matrix.[3] The lattice-like arrangement of these collagen fibrils is necessary for corneal transparency.

Fibrils organize into larger fibers or lamellae, about 1 to 2 μm thick and 10 to 200 μm wide that can traverse the entire cornea from limbus to limbus.[1] Corneal shape, which crucially defines its refractive function, is thought to be controlled by the mechanical properties of these larger collagen fibers and their three-dimensional (3-D) structural organization. As the refractive power of the cornea is controlled by its shape, the organization and biomechanics of collagen fibers are thought to play an important role in determining visual acuity.

A large body of research has been devoted to exploring the structure and biomechanics of the corneal stroma.[1,4–11] However, the mechanisms that control corneal shape remain poorly understood. Corneal structure has been studied on different levels using a variety of imaging modalities. At the molecular level, the nanostructure has been imaged using electron microscopy.[9] The spatial organization of the larger, micron-scale collagen fibers has been primarily studied using optical modalities, including fluorescence,[12] polarized light,[13] and confocal microscopy.[14,15] Additionally, x-ray diffraction has proven to be a valuable tool in determining bulk collagen orientation and alignment across the whole cornea.[1,5,6,10]

Recently, nonlinear optical imaging (NLO), primarily in the form of second harmonic generation (SHG) imaging, has emerged as a versatile and powerful tool to study the organization of corneal collagen.[7,16] Due to the nature of the second harmonic process, only fibrillar collagen emits a signal within a well-defined and highly confined focal region in the cornea. As a result, SHG allows for highly specific, 3-D imaging of corneal collagen at submicron resolution. Despite its high resolution, SHG is an optical imaging modality and is subject to the diffraction limit. It cannot resolve nanoscopic structures

such as individual collagen fibrils, which can be imaged using nonoptical imaging methodologies such as electron microscopy. Instead, SHG visualizes the aggregate signal from multiple fibrils arranged into larger fibers.

With an SHG-based imaging paradigm, we have recently created large-scale, 3-D mosaics of entire corneal cross-sections using NLO high-resolution macroscopy (HRMac).[17,18] The reconstructions identified a population of transverse-oriented collagen fibers that in the anterior stroma often originated or fused with the anterior limiting lamina (i.e., Bowman's layer).[7,19] These fibers showed a high degree of branching and intertwining with other collagen fibers which significantly decreased with stromal depth. Additionally, we found evidence of long, "anchoring" fibers that extend from the limbus into the midstroma, gradually moving anteriorly over several millimeters before branching and anastomosing with the anterior collagen fiber network. These fibers appear to directly connect the anterior central cornea with the deeper scleral layers.[19]

The absence of transverse fibers that insert into Bowman's layer in keratoconus corneas indicated that these fibers fulfill a crucial structural role in stabilizing corneal shape.[8] Reconstructions quantifying the axial heterogeneity in collagen fiber interconnectivity showed that there is a logarithmic decline in the amount of fiber branching and fusing with increasing distance from Bowman's layer, which matched a logarithmic decline in axial elastic modulus as determined by indentation and transverse shear testing.[19,20] However, the regional distribution of transverse fibers has not yet been quantified, and their role in controlling corneal shape has yet to be elucidated.

In our previous report, we quantified collagen fiber interconnectivity by determining branching point density.[19] This process relied on manually tracing fibers to find branching and fusing points, which was time consuming and labor intensive. To begin to build up a blueprint of the 3-D collagen organization of the cornea, we have developed an improved, automated approach to measure the collagen fiber angle distribution relative to the corneal surface. This new approach allows us to rapidly generate large numerical datasets that can also be incorporated into finite element models of the cornea. Linking the spatial distribution of corneal collagen in all three dimensions to the mechanical properties may allow finite element models to more accurately simulate the effects of refractive surgery or disorders, such as Keratoconus and post-LASIK ectasia.

Materials and Methods

Tissues

Autopsy eyes from three donors (aged 61–91 years) were obtained from the San Diego Eye Bank following institutional board approval and in accordance with the tenets of the Declaration of Helsinki. Eyes were fixed within 25 to 36 hours postmortem. Globes were inspected under a stereo microscope to ensure the absence of major defects or abnormalities.

Sample Preparation

Eye bank corneas generally exhibited significant swelling and crimping of collagen fibers due to the lack of pressure-induced mechanical load following the postmortem shutdown of the endothelial pump and drop in intraocular pressure (IOP). To counteract these effects, corneas were thinned prior to fixing by infusing PBS (pH 7.4) at a pressure of 50 mm Hg for 30 minutes. The increase in IOP served to restore mechanical load, which resulted in a marked straightening of collagen fibers and a reduction in corneal swelling. Corneal thickness was measured following imaging and was found to be approximately 500 μm. Eyes were then fixed under similar pressure by perfusion with 4% paraformaldehyde (PFA; Electron Microscopy Science, Hatfield, PA) in PBS. Corneal orientation was determined based on the insertion of the inferior oblique muscle. Finally, corneas were removed from the globes, taking care to preserve a thin, 1 to 2 mm rim of sclera that was cut slightly thicker at the anatomic 12 o'clock position to indicate orientation.

HRMac Imaging

Using a scalpel blade, corneas were cut into four quadrants along the vertical and horizontal meridians. Each piece was embedded vertically in low melting point agarose (NuSieve GTG, Lonza Group Ltd., Rockland, ME). Multiple consecutive slices, each approximately 300-μm thick, were cut using a vibratome (Vibratome 1500; Intracel Ltd., Shepreth, UK) and stored in 4% PFA in PBS.

NLO Imaging and Image Concatenation

Slices were imaged using our high-resolution macroscopy paradigm described in detail in our previous report.[17] Briefly, samples were placed on a glass slide under a laser scanning microscope (Zeiss 510 LSM; Carl Zeiss, Inc., Thornwood, NY) and illuminated with 150 fs laser pulses generated by laser (Chameleon Titanium Sapphire laser; Coherent, Santa Clara, CA) tuned to 820 nm. Backscattered second harmonic light at 410 nm was collected by the LSM's metadetector array.

Multiple consecutive, overlapping three-dimensional image stacks were acquired using a commercial microscopy (40×/1.2 NA Zeiss Apochromat objective; Carl Zeiss, Inc.) with increasing focal depth to a depth of approximately 80 μm. Stacks were concatenated to form a single large-scale mosaic using a combination of Java-based image plug-ins and scripts (ImageJ; National Institutes of Health, Bethesda, MD), resulting in a multi-plane HRMac.TIFF image of each slice with a lateral resolution of 0.44 μm/pixel. Each image had a size of approximately 15,000 × 5000 pixels, but varied by quadrant according to corneal diameter, radius of curvature, and orientation on the microscope.

Image Processing and Analysis

Image Processing. Image processing, analysis and visualization were carried out on a personal computer (dual Intel Xeon X5550 Quad Core; Intel, Santa Clara, CA) with central processing units clocked at 2.67 GHz per core with 32 GB of RAM running a 64-bit version of a commercial operating system (Windows 7; Microsoft Corp., Redmond, WA). Unless otherwise specified, image processing was performed with an image processing package (Fiji,[21] an ImageJ distribution; NIH), using custom-written macros.

Automated Fiber Angle Analysis. Collagen fiber angles were measured as a function of radial position (distance from the limbus) and stromal depth (distance from Bowman's layer). To account for differences in corneal shape and thickness between samples, we developed a semiautomated approach for collecting data relative to the shape of each individual quadrant as described previously.[19]

Using commercial software (MetaMorph; Molecular Devices, Sunnyvale, CA), approximately 200 landmarks each were placed along the anterior and posterior surface of the corneal reconstruction. Based on these landmarks, second-order polynomial curves were fitted to the anterior and posterior

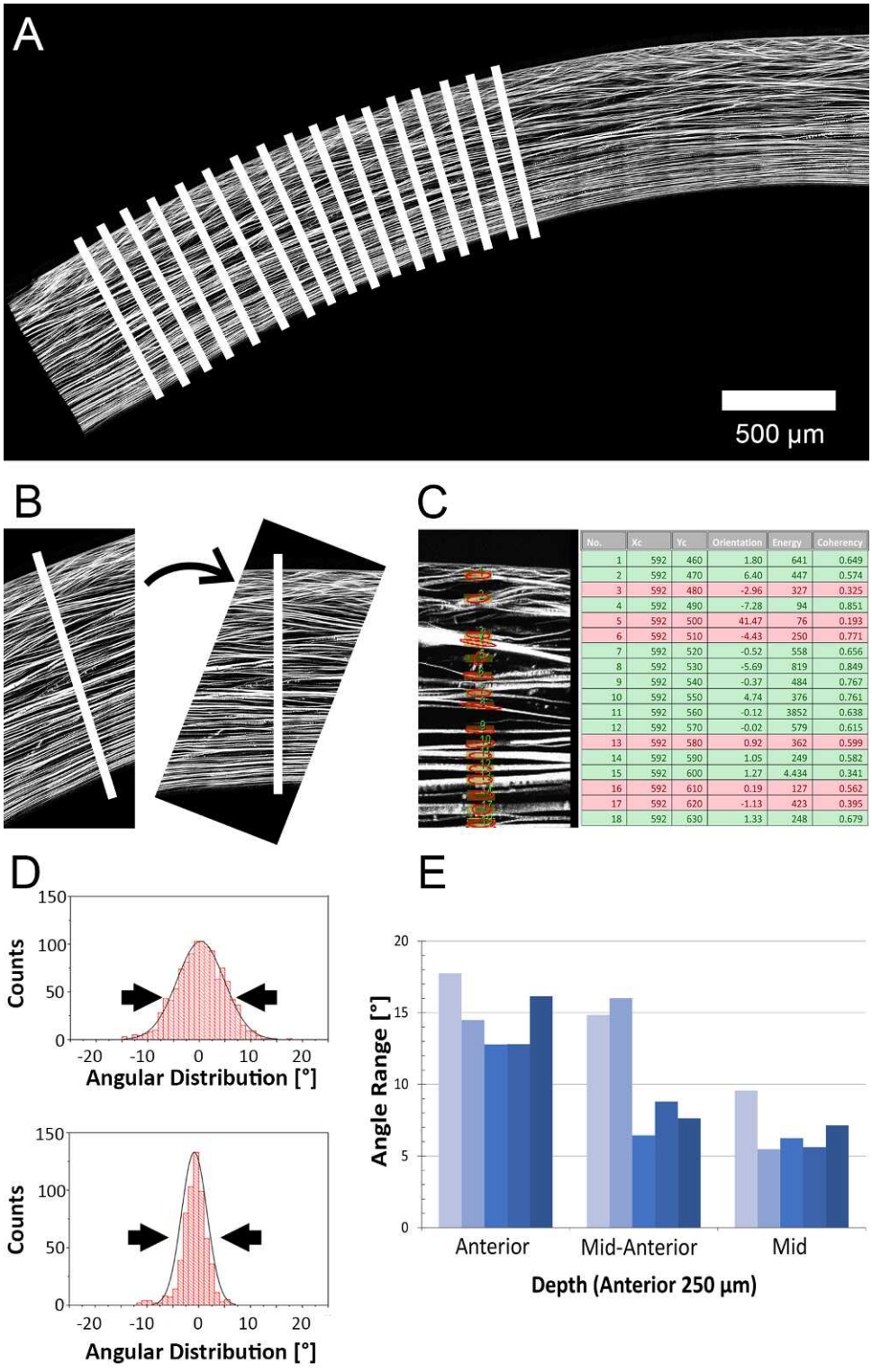

Figure 1. Image processing pipeline. (**A**) After manually designating the anterior and posterior surfaces of an HRMac image of a corneal quadrant, our software generates vertical guidelines (not drawn to scale). (**B**) At each guideline, a subimage is extracted, enlarged, and rotated to compensate for corneal curvature. (**C**) ROIs are generated along the guideline, and the predominant orientation within each ROI is measured. Energy and coherence are recorded and used to separate background noise from signal (fibers). (**D**) Angle values are grouped by stromal depth and by location and the range of angles is plotted as histograms. Gaussian curves are fitted, and the FWHM is used to determine angle ranges (*double arrows*). (**E**) FWHM and other values are plotted as a function of depth and location for each quadrant.

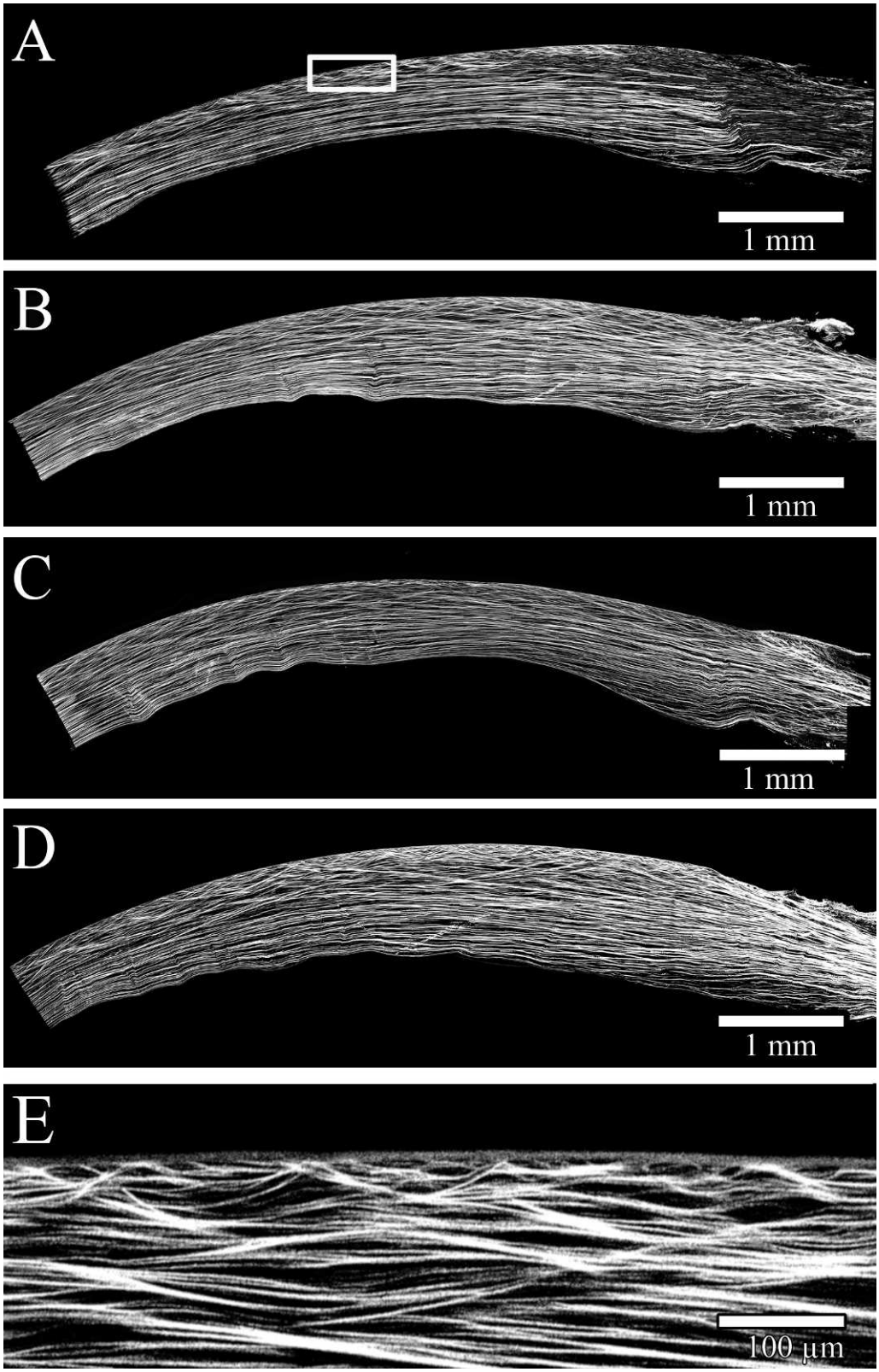

FIGURE 2. HRMac images of corneal quadrants. (**A–D**): "Zoomed-out," lower-resolution images of three quadrants allow for macroscopic assessment of curvature and macro-scale fiber patterns. (**E**) A close-up view at the full resolution of 0.44 μm/pixel allows for the inspection of individual fibers and their angles. The anterior portion is highly complex and shows considerably more branching and anastomosing than the posterior stroma.

Investigative Ophthalmology & Visual Science

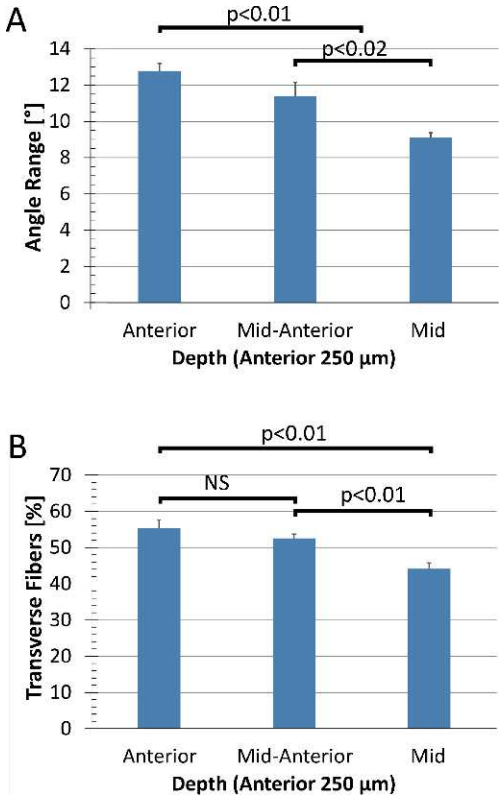

FIGURE 3. Angle range (**A**) and amount of transverse fibers (**B**) plotted as a function of stromal depth. Values were averaged over quadrants, radial positions and eyes to explore depth dependency, and divided into three equal groups of 83 µm each. There is a statistically significant drop in both angle range and transverse fibers with increasing stromal depth.

surface of HRMac image with high degrees of accuracy ($R^2 >$ 0.99). Next, custom-written software used these curves to generate virtual perpendicular guidelines along the cornea's anterior and posterior surfaces at 25-µm intervals. The guidelines were projected onto the HRMac images and were individually inspected to ensure a good fit before running the quantification algorithm (Fig. 1A).

The quantification software itself was based on the OrientationJ algorithm developed by Sage et al.,[22] which uses structure tensors to determine the orientation and isotropy of a region of interest (ROI). Our software expands its capabilities by automating the entire measurement process.

Initially, a subimage centered on the first guideline was extracted. The image was rotated so that the anterior surface of the cornea was horizontal, because OrientationJ expresses all angles relative to the horizontal direction (Fig. 1B). The subimage was enlarged by a factor of 2 to allow for a smaller, more precise ROI.

Next, a ROI centered on the guideline and measuring 25×4 µm (width by height, corresponding to radial position by stromal depth) was created, and the predominant orientation as well as its energy and coherency were measured by OrientationJ (Fig. 1C). The latter two values are measures of pixel intensity and isotropy and were used to distinguish between signal (fibers) and noise (background). All three values were recorded along with position information for the rectangle, and the ROI was moved downward by 3 µm for the next measurement until the posterior surface of the cornea was reached. As the ROI measured 4 µm in height, this caused oversampling, ensuring that all fibers were measured and accounted for. Finally, the subimage was saved before closing for troubleshooting purposes.

This process was repeated for each guideline, resulting in approximately 200 subimages per quadrant, yielding well over 30,000 data points per corneal section. The data from all images was written to a file in comma-separated value (csv) format.

The .csv files were imported into a spreadsheet program (Microsoft Excel 2010; Microsoft Corp.). False positives, caused by the software determining orientation of background noise or from very weak fibers, were filtered out by removing all values that did not match empirically determined thresholds for energy and coherency. Thresholds were adjusted on a per-scan basis according to average image intensity for energy, while the cutoff value for coherency was based on previously published values.[22] To validate these threshold settings, fiber angles were manually measured in a small volume by three different operators to minimize bias. These manually obtained values were found to be in good agreement with the results from the automated algorithm. Because our previous study showed that the overwhelming majority of angled fibers are found in the anterior cornea, and due to the fact that swelling predominantly occurs in the posterior cornea,[23] we restricted our analysis to the anterior 250 µm. This markedly reduced the amount of false positives due to wavy fibers caused by swelling.

The filtered values for each quadrant were equally distributed into five radial regions from the center to periphery. Regions were 1.3-mm wide on average and varied with corneal diameter. Within each region, values from the anterior 250 µm were further subdivided by depth into three equal groups of 83 µm. Two separate types of plots were generated: angle range and transverse versus parallel fibers. Both types were statistically tested for significant interactions between eyes, regions and quadrants.

To determine angle range, angle values were plotted as histograms using graphing software (Origin; OriginLab, Northampton, MA). A Gaussian curve was fit to the distribution, and the full width at half maximum (FWHM) of these curves were plotted (Fig. 1D). Regions with largely parallel fiber angles had a low FWHM, whereas those with a wide variety of fiber angles were characterized by high FWHM values.

The percentage of transverse fibers was defined as the percentage of fibers that do not follow corneal curvature (i.e., those that run at an angle to the corneal surface, which was set at an angle of 0°). To account for minor inaccuracies in determining the 0 angle, fibers were counted as being transverse rather than parallel if they deviated by more than ±3.5°. Fiber angle range was plotted as a function of depth and radial position (Fig. 1E). Similar plots as functions of anatomical quadrant and radial position were generated for both fiber angle range and transverse fiber percentage.

Statistical Analysis

Statistical analysis was carried out in statistical software (SigmaStat 3.4; Systat Software, San Jose, CA). Three-way analysis of variance was performed on datasets using the Holm-Sidak method.

RESULTS

Representative NLO-HRMac images of different corneal quadrants are shown in Figure 2. Each image was analyzed separately and yielded more than 250,000 data points for all four quadrants per eye before filtering. By removing false positives and noise, about 30,000 angle values were extracted

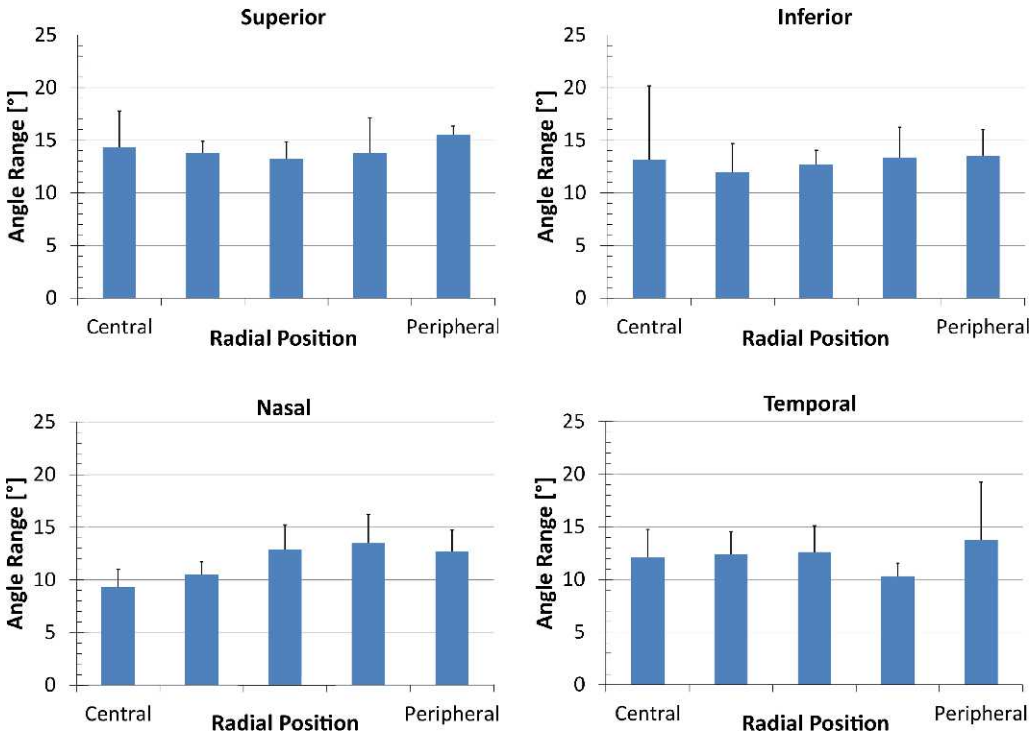

FIGURE 4. Fiber angle range plotted for each quadrant by radial position going from the central cornea ("*Central*") to the limbus ("*Peripheral*"). There is no statistically significant difference between radial positions or quadrants.

for each eye, or about 7500 values per quadrant. Approximately 500 data points contributed to each angle range value.

Average fiber angle range of all three eyes was plotted as a function of depth (Fig. 3A). There was a statistically significant reduction ($P < 0.02$) in fiber angle range with increasing distance from the anterior surface. The variation between individual eyes was not significant ($P > 0.1$). There was a corresponding reduction in transverse fiber percentage (Fig. 3B), though the difference between the anterior and the middle segments was not significant ($P > 0.05$).

Transverse fibers generally ran at shallow angles, with some steeper angles found closer to the anterior surface. When analyzed as a function of depth, 95% of angles were found to be within $\pm 11°$ (anterior), $\pm 9.1°$ (anterior-mid), and $\pm 8.1°$ (mid) relative to the corneal surface.

To compare angle range and transverse fiber percentage radially, results from the anterior stroma were plotted by region for each quadrant for fiber angle range (Fig. 4) and transverse fiber fraction (Fig. 5). Fiber angle range varied between eyes, quadrants and regions, but showed no statistically significant differences. The transverse fiber percentage included comparable amounts of variation. However, a statistically significant difference between the superior and nasal quadrants was found (Fig. 5). No significant difference was found between radial position or between eyes.

The results of the ANOVA tests for angle range and transverse fiber fraction are shown in Table 1. With the exception of the depth dependency, there were no significant differences in angle range between eyes, radial position, meridians or quadrants. The transverse fiber percentage shows a significant difference between the superior and nasal quadrant, but no significant difference between eyes or radial positions.

Raw values for the fiber angle range as a function of depth, radial position, and quadrant averaged over all three eyes were can be seen in Table 2.

DISCUSSION

To begin to develop a "blueprint" of collagen fiber organization of the human cornea, we have developed a method for rapid quantification of collagen fiber angle distribution in corneal cross-sections and have applied it to human eyes. Our results confirm a depth-dependent decrease in organizational complexity, but found no significant radial variation in fiber organization. The resulting datasets provide real-world input for finite element models of human corneas.

The reduction in fiber angle range and transverse fiber percentage with increasing stromal depth matches the reduction in branching point density observed previously.[19] Since any branching point consists of two divergent fibers, at least one fiber necessarily is angled relative to the corneal surface. As such, the fiber angle distribution was expected to drop with increasing stromal depth.

No significant trends were found in the radial distribution of fiber angles. In addition to comparing all four quadrants individually, data was grouped to compare the nasal/temporal and superior/inferior meridians, as well as central and peripheral cornea. In most cases, there was no statistically significant difference in either fiber angle range or transverse fibers. The one notable exception was a significant difference in the amount of transverse fibers between the superior and nasal quadrants. While statistically significant, the difference was small (<8%) and unlikely to affect overall corneal biomechanics. There did not appear to be an immediately obvious physiological explanation for, or the effect of, this minor difference.

We have previously established a link between stromal collagen fiber branching and mechanical stiffness.[19] Therefore, the absence of any detectable trend in radial fiber distribution indicates a lack of significant variations in stiffness between different corneal quadrants in apparently normal eyes. This likely serves to evenly distribute stresses, avoiding the

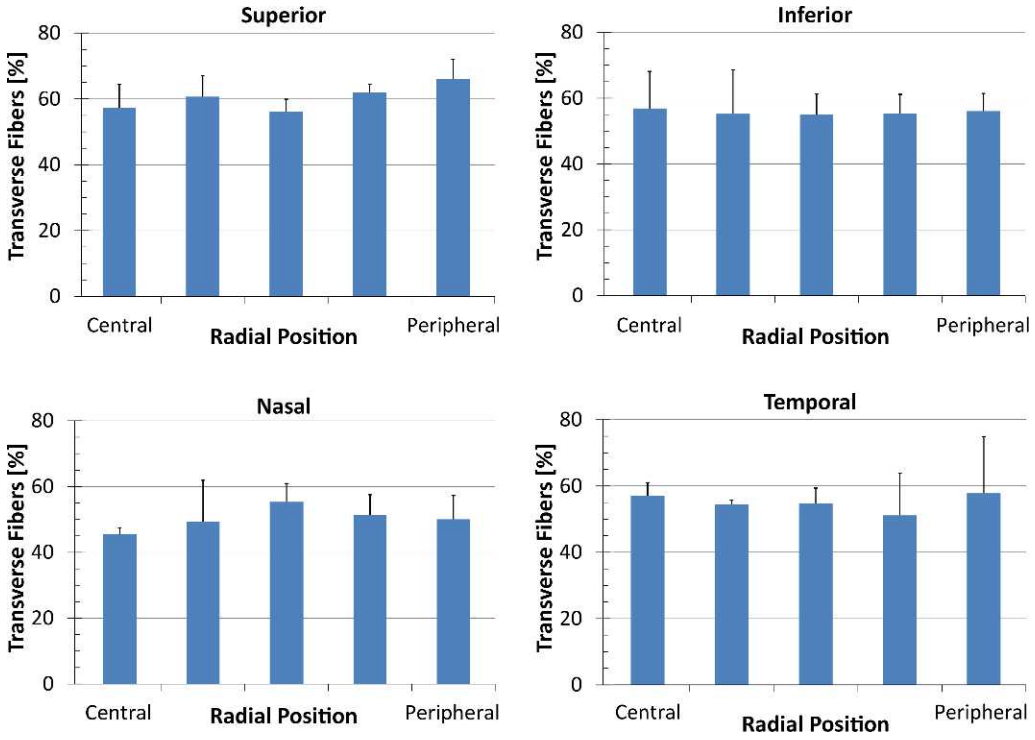

FIGURE 5. Transverse fiber amounts plotted for each quadrant by radial position going from the central cornea ("*Central*") to the limbus ("*Peripheral*"). There is no statistically significant difference between radial positions; however, a significant difference was found between the superior and the nasal quadrants.

formation of regions of increased stress, which are more susceptible to deformation or failure. Since earlier studies of keratoconus corneas have shown a loss of angled fibers in the anterior stroma, particularly those connecting to Bowman's layer, it is possible that corneas with abnormal corneal shapes, such as astigmatic cornea, might show similar regional variations related to corneal steepening or flattening. Certainly additional studies of the corneal structure using this automated approach are needed to evaluate this possibility.

Though seemingly almost random, the observed distribution of fiber angles likely serves an important purpose. The result of this particular distribution of fiber angles is the absence of preferred collagen fiber directions in the anterior stroma. This matches observations by Quantock et al. using small angle x-ray scattering.[24] A similar lack of a preferred directionality of in-plane fibers in the anterior cornea when viewed en face has been shown by Meek et al. using x-ray diffraction.[5] In the posterior stroma, however, a large amount of collagen fiber bundles are oriented along two preferred orientations.[4] Our observation of fiber angle distributions that show no preferred regions in the anterior stroma and the reduction of transverse fibers toward the posterior stroma appears to be the continuation of this trend into the third dimension.

Overall, the human corneal stroma appears to be divided into two main structural zones. The posterior region is primarily composed of very regular layers of collagen fibers aligned parallel to the corneal surface and oriented predominantly along the superior/inferior and nasal/temporal meridians along with a circular alignment in the peripheral cornea. Due to markedly reduced connections between adjacent layers, this region is likely vulnerable to slippage of fibers. As a result of the high degree of fiber alignment, stress would be concentrated at the superior, inferior, nasal, and temporal limbus where radially oriented fibers merge with more circumferentially oriented collagen at the corneoscleral interface. By itself, we expect this type of fiber organization to be unstable, vulnerable to fiber slippage and ectasia similar to keratoconus.

In the anterior stroma, collagen fiber organization is much more random, within limits. A large quantity of transverse fibers can be found especially close to the anterior surface. These fibers connect not just adjacent layers, but often run across multiple layers, branching several times and in many cases inserting into Bowman's layer with no preferred in-plane orientation of fibers. Consequently, the anterior stroma is highly interconnected, making it more mechanically stable against shear forces[20] and increasing stiffness.[19] This suggests that the anterior stroma plays a stabilizing role atop the posterior region, which is likely more susceptible to these forces. The seeming randomness of the anterior stroma may therefore represent a mechanism to stabilize the cornea through an even distribution of forces due to a lack of preferred angles, while simultaneously maintaining a high degree of interconnectivity between fibers to avoid slippage.

TABLE 1. List of Interactions Tested

Interaction	Angle Range	Transverse Fiber Fraction
Eyes	None	None
Radial position	None	None
Meridians	None	None
Quadrants	None	Superior/nasal
Depth	Anterior/mid-anterior, mid Anterior/mid-anterior/mid	Anterior/mid, mid Anterior/mid

Two- and three-way ANOVA tests using the Holm-Sidak method were run to look for significant differences in angle range and transverse fiber fraction.

Table 2. Fiber Angle Range by Quadrant

		Radial Position					
Quadrant	**Depth**	**1**	**2**	**3**	**4**	**5**	**Average**
Superior	Ant	14.30 ± 3.48	13.81 ± 1.07	13.26 ± 1.58	13.82 ± 3.30	15.53 ± 0.82	14.14 ± 2.05
	Mid-ant	12.61 ± 2.10	12.35 ± 3.18	12.39 ± 5.17	12.83 ± 4.22	8.76 ± 1.88	11.79 ± 1.78
	Mid	8.90 ± 1.76	8.66 ± 3.09	10.95 ± 4.54	9.88 ± 3.96	8.03 ± 1.91	9.29 ± 3.05
Inferior	Ant	14.38 ± 5.77	10.69 ± 3.60	12.88 ± 1.60	12.99 ± 2.43	13.97 ± 2.08	12.98 ± 3.10
	Mid-ant	11.06 ± 0.95	13.31 ± 2.50	11.35 ± 1.52	12.41 ± 2.30	11.24 ± 2.57	11.87 ± 1.97
	Mid	9.24 ± 2.68	8.85 ± 1.57	8.62 ± 3.36	10.89 ± 4.20	7.98 ± 2.41	9.12 ± 2.85
Nasal	Ant	10.70 ± 1.31	11.77 ± 3.35	12.89 ± 2.32	12.25 ± 2.03	11.28 ± 3.71	11.78 ± 2.54
	Mid-ant	12.24 ± 2.99	9.22 ± 2.15	10.77 ± 1.34	11.40 ± 1.85	9.65 ± 3.04	10.65 ± 2.27
	Mid	8.33 ± 1.81	9.54 ± 1.93	7.62 ± 2.22	8.85 ± 3.90	8.54 ± 3.32	8.58 ± 2.64
Temporal	Ant	12.11 ± 2.65	12.40 ± 2.15	12.62 ± 2.49	10.32 ± 1.24	13.75 ± 5.51	12.24 ± 2.81
	Mid-ant	12.28 ± 2.95	12.80 ± 2.11	11.11 ± 1.26	10.20 ± 2.01	9.91 ± 1.13	11.26 ± 1.89
	Mid	10.96 ± 3.42	9.50 ± 1.75	11.38 ± 2.80	7.52 ± 1.73	8.04 ± 1.18	9.48 ± 2.17

Ant, anterior; mid-ant, mid-anterior. Radial position going from central cornea (1) to the limbus (5) and depth averaged over all three eyes.

We infer that the branching leads to increased stiffness and that the lack of branching in keratoconus[8] could be related to increased corneal compliance. This reduction in transverse fibers would then imply that in corneas with keratoconus, the anterior stroma is markedly less effective at stabilizing corneal biomechanics. Keratoconus has been hypothesized to involve fiber slippage,[25–27] and we presume that transverse fibers may play a role in this process. Corneas lacking a sufficient number of stabilizing transverse fibers would be more susceptible to slippage and the subsequent development of the characteristic cone.

Corneas are known to remain stable even after a sizeable fraction of the anterior cornea, and the transverse fibers it contains, has been disrupted or ablated, such as in LASIK or photorefractive keratectomy. On the other hand, excessive removal of the anterior stroma beyond the minimum residual bed thickness can lead to post-LASIK ectasia. Interestingly, this suggests that anterior stroma in adult eyes is considerably stronger than necessary to stabilize the human cornea, perhaps in part due to the known increasing stiffness of the cornea with age, associated with natural collagen crosslinking.[28] A possible interpretation is that during neonatal development, the collagen fiber branching establishes a scaffold to maintain corneal shape. Natural collagen crosslinking likely leads to increased tensile stiffness of collagen fibers, which would allow mature corneas to rely less on transverse and branched fibers to maintain stability. The scaffold topology would therefore become less crucial in stabilizing corneal shape over time. This would enable mature corneas to retain corneal shape even when missing significant portions of the anterior stroma following refractive surgery. Based on the high success rates, we can infer that in mature eyes, this reduction in transverse fibers is unlikely to affect corneal biomechanics in a way that would cause a destabilization of corneal shape.

As more microstructural features of the stroma have been discovered and measured over the past decades, increasingly complex mathematical models have been developed to incorporate these findings. Such models, when used in combination with experimentally determined tissue mechanical properties, help explain the relationship between the structural organization of the cornea and its shape. The finite element method provides a particularly elegant and flexible computational framework in which to implement these mathematical models. For example, models have taken into account the spatial distribution of stromal collagen to various degrees,[29–32] and different mathematical approaches have been used to incorporate the preferential in-plane alignment of collagen fibers measured by x-ray scattering.[1] While representing a significant improvement over earlier efforts, these models have neglected the effects of transverse fibers or depth-dependent variation of the tissue organization. The depth-dependence of the stromal collagen distribution shown by both SHG[8,19] and x-ray scattering performed on corneal flaps[4] was not being taken into account, leaving the opportunity for further enhancement of the represented three-dimensional collagen architecture in human cornea models.

Imaging has shown this axial heterogeneity for some time, and the corresponding characterization of corneal biomechanical properties has recently been undertaken.[19,20,33] To the best of our knowledge, the depth-dependent angular distribution of transverse collagen fibers has only been implemented in a single finite element model thus far.[34] While this model correctly accounts for the three-dimensional collagen architecture of the cornea, simplifying assumptions have been made in constructing the model due to the lack of available real-world data. In principle, the finite element method is well-adapted to describe the full 3-D tissue organization and mechanical behavior, and its primary limitation in practice is the availability of suitably detailed quantitative data. To accurately simulate corneal biomechanics, more realistic finite element models are needed.

The automated approach to quantifying transverse fiber angles presented here allows for the generation of fiber distribution data that can be used to improve finite element models of corneas. The three-dimensional distributions measured in this study can be directly implemented into a computational model with the finite element method. When full three-dimensional architecture and microstructure are modeled, finite element analysis can be used to more accurately explore the effects of compromised corneal architecture as in the case of keratoconus or post-LASIK surgery. Such models can also be used to inexpensively test possible new therapeutic approaches that rely on modifying corneal biomechanics, such as riboflavin-induced corneal crosslinking.

In summary, our study confirms earlier observations that collagen fiber interconnectivity is dependent on stromal depth. Based on our data, we hypothesize that transverse fibers play an important role in determining corneal biomechanics and shape. The lack of a significant difference in fiber angle range with regard to either radial position or corneal quadrant suggests that loads are evenly distributed, stabilizing corneal shape. The high degree of interconnectivity between stromal layers as evidenced by transverse fibers is most pronounced in the anterior stroma, which likely serves to stabilize shape and

to prevent fiber slippage. Further studies exploring the relationship between corneal topography and transverse fiber distribution may elucidate the underlying mechanisms of abnormal corneal biomechanics (i.e., astigmatism and keratoconus).

Acknowledgments

Parts of this study were presented at the annual meeting of the Association for Research in Vision and Ophthalmology, Fort Lauderdale, Florida, May 2012.

Supported by NIH Grants EY018665 and EY019719, The Discovery Eye Foundation, The Skirball Program in Molecular Ophthalmology, and a grant from Research to Prevent Blindness, Inc. The authors alone are responsible for the content and writing of the paper.

Disclosure: **M. Winkler**, None; **G. Shoa**, None; **Y. Xie**, None; **S.J. Petsche**, None; **P.M. Pinsky**, None; **T. Juhasz**, None; **D.J. Brown**, None; **J.V. Jester**, None

References

1. Meek KM, Boote C. The use of x-ray scattering techniques to quantify the orientation and distribution of collagen in the corneal stroma. *Prog Retin Eye Res*. 2009;28:369–392.
2. Daxer A, Misof K, Grabner B, Ettl A, Fratzl P. Collagen fibrils in the human corneal stroma: structure and aging. *Invest Ophthalmol Vis Sci*. 1998;39:644–648.
3. Quantock AJ, Young RD. Development of the corneal stroma, and the collagen–proteoglycan associations that help define its structure and function. *Dev Dyn*. 2008;237:2607–2621.
4. Abahussin M, Hayes S, Cartwright NEK, et al. 3D collagen orientation study of the human cornea using x-ray diffraction and femtosecond laser technology. *Invest Ophthalmol Vis Sci*. 2009;50:5159–5164.
5. Aghamohammadzadeh H, Newton RH, Meek KM. X-ray scattering used to map the preferred collagen orientation in the human cornea and limbus. *Structure*. 2004;12:249–256.
6. Meek KM, Boote C. The organization of collagen in the corneal stroma. *Exp Eye Res*. 2004;78:503–512.
7. Morishige N, Petroll WM, Nishida T, Kenney MC, Jester JV. Noninvasive corneal stromal collagen imaging using two-photon-generated second-harmonic signals. *J Cataract Refract Surg*. 2006;32:1784.
8. Morishige N, Wahlert AJ, Kenney MC, et al. Second-harmonic imaging microscopy of normal human and keratoconus cornea. *Invest Ophthalmol Vis Sci*. 2007;48:1087–1094.
9. Komai Y, Ushiki T. The three-dimensional organization of collagen fibrils in the human cornea and sclera. *Invest Ophthalmol Vis Sci*. 1991;32:2244–2258.
10. Boote C, Hayes S, Abahussin M, Meek KM. Mapping collagen organization in the human cornea: left and right eyes are structurally distinct. *Invest Ophthalmol Vis Sci*. 2006;47:901–908.
11. Borcherding MS, Blacik L, Sittig R, Bizzell JW, Breen M, Weinstein H. Proteoglycans and collagen fibre organization in human corneoscleral tissue. *Exp Eye Res*. 1975;21:59–70.
12. Konomi H, Hayashi T, Nakayasu K, Arima M. Localization of type V collagen and type IV collagen in human cornea, lung, and skin. Immunohistochemical evidence by anti-collagen antibodies characterized by immunoelectroblotting. *Am J Pathol*. 1984;116:417.
13. Stanworth A, Naylor E. Polarized light studies of the cornea I. The isolated cornea. *J Exp Biol*. 1953;30:160–163.
14. Hahnel C, Somodi S, Weiss DG, Guthoff RF. The keratocyte network of human cornea: a three-dimensional study using confocal laser scanning fluorescence microscopy. *Cornea*. 2000;19:185.
15. Jalbert I, Stapleton F, Papas E, Sweeney D, Coroneo M. In vivo confocal microscopy of the human cornea. *Br J Ophthalmol*. 2003;87:225–236.
16. Han M, Giese G, Bille J. Second harmonic generation imaging of collagen fibrils in cornea and sclera. *Opt Express*. 2005;13:5791–5797.
17. Jester JV, Winkler M, Jester BE, Nien C, Chai D, Brown DJ. Evaluating corneal collagen organization using high-resolution nonlinear optical macroscopy. *Eye Contact Lens*. 2010;36:260–264.
18. Winkler M, Jester BE, Nien-Shy C, Chai D, Brown DJ, Jester JV. High resolution macroscopy (HRMac) of the eye using nonlinear optical imaging. *Proc SPIE*. 2010;7589:758906.
19. Winkler M, Chai D, Kriling S, et al. Nonlinear optical macroscopic assessment of 3-D corneal collagen organization and axial biomechanics. *Invest Ophthalmol Vis Sci*. 2011;52:8818–8827.
20. Petsche SJ, Chernyak D, Martiz J, Levenston ME, Pinsky PM. Depth-dependent transverse shear properties of the human corneal stroma. *Invest Ophthalmol Vis Sci*. 2012;53:873–880.
21. Schindelin J, Arganda-Carreras I, Frise E, et al. Fiji: an open-source platform for biological-image analysis. *Nature Methods*. 2012;9:676–682.
22. Rezakhaniha R, Agianniotis A, Schrauwen JT, et al. Experimental investigation of collagen waviness and orientation in the arterial adventitia using confocal laser scanning microscopy. *Biomech Model Mechanobiol*. 2012;11:461–473.
23. Müller LJ, Pels E, Vrensen GF. The specific architecture of the anterior stroma accounts for maintenance of corneal curvature. *Br J Ophthalmol*. 2001;85:437–443.
24. Quantock AJ, Boote C, Young RD, et al. Small-angle fibre diffraction studies of corneal matrix structure: a depth-profiled investigation of the human eye-bank cornea. *J Appl Crystallogr*. 2007;40:335–340.
25. Meek KM, Tuft SJ, Huang Y, et al. Changes in collagen orientation and distribution in keratoconus corneas. *Invest Ophthalmol Vis Sci*. 2005;46:1948–1956.
26. McMonnies CW. Mechanisms of rubbing-related corneal trauma in keratoconus. *Cornea*. 2009;28:607–615.
27. Tan H-Y, Sun Y, Lo W, et al. Multiphoton fluorescence and second harmonic generation imaging of the structural alterations in keratoconus ex vivo. *Invest Ophthalmol Vis Sci*. 2006;47:5251–5259.
28. Elsheikh A, Wang D, Brown M, Rama P, Campanelli M, Pye D. Assessment of corneal biomechanical properties and their variation with age. *Curr Eye Res*. 2007;32:11–19.
29. Pinsky PM, van der Heide D, Chernyak D. Computational modeling of mechanical anisotropy in the cornea and sclera. *J Cataract Refract Surg*. 2005;31:136–145.
30. Grytz R, Meschke G. A computational remodeling approach to predict the physiological architecture of the collagen fibril network in corneo-scleral shells. *Biomech Model Mechanobiol*. 2010;9:225–235.
31. Studer H, Larrea X, Riedwyl H, Büchler P. Biomechanical model of human cornea based on stromal microstructure. *J Biomech*. 2010;43:836–842.
32. Holzapfel GA. Three-dimensional modeling and computational analysis of the human cornea considering distributed collagen fibril orientations. *J Biomech Eng*. 2008;130:061006–061001.
33. Sondergaard AP, Ivarsen A, Hjortdal J. Reduction of stromal swelling pressure after UVA-riboflavin cross-linking. *Invest Ophthalmol Vis Sci*. 2013;54:1625–1634.
34. Petsche SJ, Pinsky PM. The role of 3-D collagen organization in stromal elasticity: a model based on x-ray diffraction data and second harmonic-generated images [published online ahead of print January 4, 2013]. *Biomech Model Mechanobiol*. doi:10.1007/s10237-012-0466-8

Investigative Ophthalmology & Visual Science